Transport properties of vortex matter governed by the edge inductance in superconducting $Bi_2Sr_2CaCu_2O_8$ crystals

H. Beidenkopf,[1,*] Y. Myasoedov,[1] E. Zeldov,[1] E. H. Brandt,[2] G. P. Mikitik,[2,3] T. Tamegai,[4] T. Sasagawa,[5] and C. J. van der Beek[6]

[1]*Department of Condensed Matter Physics, Weizmann Institute of Science, Rehovot 76100, Israel*

[2]*Max-Planck-Institut für Metallforschung, Heisenbergstr. 3, D-70506 Stuttgart, Germany*

[3]*B. Verkin Institute for Low Temperature Physics & Engineering, Kharkov 61103, Ukraine*

[4]*Department of Applied Physics, The University of Tokyo, Hongo, Bunkyo-ku, Tokyo 113-8656, Japan*

[5]*Materials and Structures Laboratory, Tokyo Institute of Technology, Kanagawa 226-8503, Japan*

[6]*Laboratoire des Solides Irradiées, CNRS UMR 7642 and CEA/IRAMIS/DRECAM, Ecole Polytechnique, 91128 Palaiseau Cedex, France*

(Received 18 October 2009; revised manuscript received 7 December 2009; published 31 December 2009)

We study the distribution of transport current across superconducting $Bi_2Sr_2CaCu_2O_8$ crystals and the vortex flow through the sample edges. We show that the T_x transition is of electrodynamic rather than thermodynamic nature, below which vortex dynamics is governed by the edge inductance instead of the resistance. This allows measurement of the resistance down to 2 orders of magnitude below the transport noise. By irradiating the current contacts the resistive step at vortex melting is shown to be due to loss of *c*-axis correlations rather than breakdown of quasilong-range order within the *a-b* planes.

DOI: 10.1103/PhysRevB.80.224526 PACS number(s): 74.25.Fy, 74.25.Bt, 74.25.Dw, 74.72.Hs

Numerous phase transitions have been proposed to interpret the intricate *B-T* phase diagram of the vortex matter in the high-temperature superconductor $Bi_2Sr_2CaCu_2O_8$ (BSCCO).[1,2] The first-order melting at T_m, that separates a quasiordered vortex solid from a vortex liquid, is widely accepted to be a genuine thermodynamic phase transition.[3–5] Experiments indicate that the glass line, T_g, is another thermodynamic transition that apparently separates amorphous solid from liquid at high fields[6–9] and Bragg glass from weakly pinned lattice at low fields.[8,9]

On the other hand, the T_x transition, which resides above T_m and T_g, has remained highly controversial. Fuchs *et al.*[10] raised the possibility that T_x has a thermodynamic origin after identifying a sharp change in the vortex transmittance through the sample edges, reflected in the current distribution across the sample. It thus suggested existence of a novel phase between T_g and T_x which was argued to be of an intermediate degree of order such as a disentangled liquid[11] or a decoupled solid,[12,13] soft solid,[14] or supersolid.[15,16] Susceptibility[3] and Josephson plasma resonance[17,18] data indicated that interplane vortex correlations are lost already across the melting transition ruling out the identification of T_x as a decoupling transition into a pancake vortex gas. The experimental evidence thus seemed to be in support of a decoupled solid phase in which the pancake vortices within each plane still retain a certain degree of order which is lost above T_x.[19–22] At the same time, theoretical studies[23,24] and numerical simulations[25,26] argued that below T_x resides a soft glassy phase with some degree of order.

In this paper we show, however, that the experimental T_x line does not represent a thermodynamic transformation of a bulk vortex property but rather reflects an *electrodynamic* crossover in the dynamic response of the sample *edges*. The inductance of the sample edges, though immeasurably low, completely governs the vortex dynamics below T_x. We use this finding to investigate the resistance due to vortex motion down to 2 orders of magnitude below the typical sensitivity of transport measurements.

The resistances of several BSCCO single crystals typically of $1500\times350\times20$ μm^3 in a dc magnetic field, $H_{dc}\|c$ axis, were measured using two complimentary techniques: directly via transport and indirectly by determining the ac current distribution with Biot-Savart law from the self-induced ac magnetic field profile. The magnetic field is measured locally with an array of 10×10 μm^2 GaAs Hall sensors. In addition, to eliminate the *c*-axis contribution to the measured resistance we irradiated the current contacts at the Grand Accélérateur National d'Ions Lourds (Caen, France) with a fluence of 2.5×10^{10} cm^{-2} 1 GeV Pb ions (matching dose of $B_\Phi=0.5$ T) while masking the central region of the sample, which remained pristine.

Figure 1(a) shows the temperature dependence of the in-phase current-induced ac field, $B^{(1)}(x)$. At high temperatures the current flows uniformly across the width of the sample both above and below T_c. Accordingly, $B^{(1)}(x)$ measured by the Hall sensors across the sample [Fig. 1(c), dots] fits precisely to that calculated via Biot-Savart law (solid line) for a uniform current distribution $j^{(1)}(x)$ [Fig. 1(c), upper panel]. We note in passing that right at T_c some small deviations in current distribution are usually observed apparently due to small sample inhomogeneities as seen in Fig. 1(c) at 85 K.

With cooling $B^{(1)}(x)$ gradually flattens out, becomes completely flat at T_{sb} and eventually inverted at yet lower temperatures. The inverted $B^{(1)}(x)$ profile is associated with essentially pure edge currents [Fig. 1(f)]. The Bean-Livingston surface barrier[27] and the platelet sample geometry[28] impose an energetic barrier that progressively impedes vortex passage through the edges with cooling. This defines an effective edge resistance, $R_e(T)$, that decreases rapidly with cooling. Below T_{sb} the edge resistance, $R_e(T)$, becomes smaller than the bulk resistance $R_b(T)$. As a result, most of the current shifts from the bulk, where little force is required to move vortices across, toward the edges, where it facilitates the hindered vortex entry and exit.[10,29,30] Bulk vortex pinning becomes dominant only at significantly lower temperatures

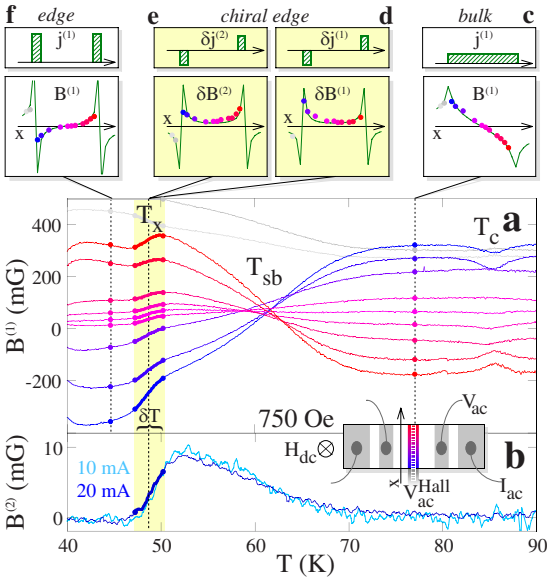

FIG. 1. (Color online) Hall sensor array measurement of the ac magnetic field self-induced by a 15 mA, 73 Hz ac current in BSCCO crystal A. (a) First harmonics of individual sensors. (b) Second harmonics from a sensor close to the edge at two current amplitudes normalized to 10 mA. (c)–(f) Magnetic profiles measured (●) and calculated (solid lines) from current profiles (upper panels) using the Biot-Savart law: (c) uniform bulk flow at high temperatures turns to (f) edge flow at low temperatures. Chiral edge flow vanishes at T_x from (d) first and (e) second harmonics. Inset in (b): schematic location of Hall sensors relative to the contacted sample.

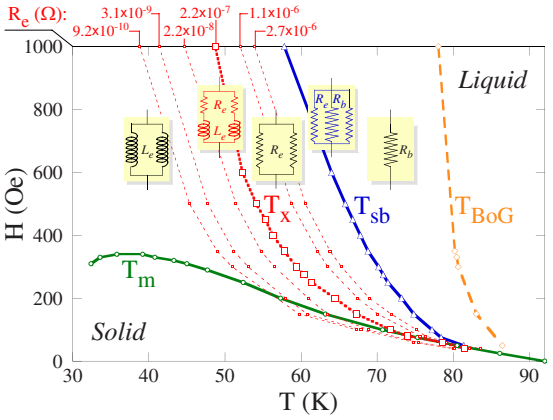

FIG. 2. (Color online) High-temperature phase diagram of the vortex matter in BSCCO crystal B. T_m is the first-order melting (○). Below T_{sb} (△) the edges shunt most of the current from the bulk while below the frequency-dependent T_x (□) the edge impedance becomes predominantly inductive. Ion-irradiated regions exhibit the Bose-glass transition, T_{BoG} (◇), below which vortices are pinned to columnar defects. The dotted lines represent equal edge-resistance contours extracted from the frequency and field dependences of T_x.

as the glass line T_g is approached (not shown).

The dynamic properties of the surface barriers have two types of asymmetries. We show that both these asymmetries modify the current distribution in the sample but do so only above T_x. One barrier asymmetry arises from the two opposite edges of the sample generally having somewhat different microscopic imperfections. It leads to different edge resistances and therefore asymmetric current distribution between the right and left edges. The T_x line, situated below T_{sb} (Fig. 2), marks the temperature below which the trace of this right-left asymmetry in the current distribution sharply disappears and the current distributes symmetrically between the edges. The perfectly symmetric edge-current distribution induces a perfectly antisymmetric magnetic field profile [Fig. 1(f)]. Hence, a small antisymmetric current component $\delta j^{(1)}$ [Fig. 1(d)], that was present above T_x, vanish below it together with its induced small symmetric contribution $\delta B^{(1)}(x) = B^{(1)}(x, T_x + \frac{\delta T}{2}) - B^{(1)}(x, T_x - \frac{\delta T}{2})$ to the otherwise antisymmetric $B^{(1)}(x)$.

The magnitude of this type of barrier asymmetry is sample dependent and may even be absent in samples with symmetric edge structure.[29] On the contrary, the second type of asymmetry arises from the asymmetry between a harder vortex entry and an easier exit through the edges, which is an inherent property of the surface barriers close to equilibrium magnetization.[27,31,32] Since the vortex entry and exit sides swap during the ac cycle, this asymmetry gives rise to a unique chiral second-harmonic edge current, $\delta j^{(2)}$, and to the corresponding second-harmonic signal $\delta B^{(2)}(x)$ shown in Fig. 1(e). It builds up gradually upon cooling [Fig. 1(b)] until it pinches off sharply at T_x [hereinafter determined at half of the $B^{(2)}(x)$ roll-off]. Accordingly, T_x marks the temperature below which the vortex flow turns insensitive to both the entry-exit and the right-left asymmetries of the surface barriers.

The T_x transition was commonly ascribed to the advent of a new vortex phase with an intermediate degree of order.[10,23–26] We show that T_x has rather electrodynamic nature, arising from the inductance of the sample edges. Following Ref. 33 we model the vortex dynamics by equivalent electric circuit with three parallel channels—the bulk and two edges. Our measurements show no dependence on the current magnitude [Fig. 1(b), dark versus pale lines]. Therefore, out of the possible models considered in Ref. 33 we follow the Ohmic one. The model assigns each channel geometrical self-inductance and mutual inductance in series to their temperature-dependent resistances.

The sample inductance is usually disregarded since it is immeasurably small in direct transport measurements. Nevertheless, it does affect the current distribution in the sample. The self-inductance and mutual inductance of the edges, as opposed to the edge resistance, are temperature independent and dictated solely by the geometry of the sample and its effective edges. Relevant for the current distribution is the combination of inductances calculated in Ref. 33 $L_e = (\mu_0/4\pi)l[\ln(2w/d)+1/4]$, where l, w, and d are the sample's length, width, and thickness, respectively. Note, that in this expression for the effective edge inductance the logarithmic divergence with the sample length cancels out.[33] For simplicity, we neglect here the kinetic inductance of the edges because it is expected to be lower by a factor $\sim\lambda/d$ than geometric inductance, where $\lambda \approx 0.2$ μm is the penetration depth.

Within this model T_x is the temperature below which the

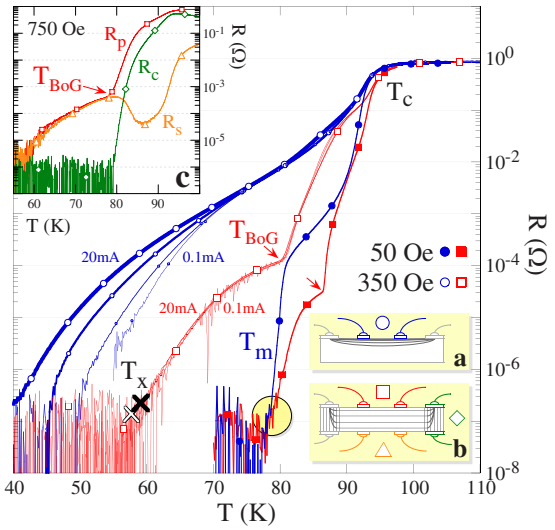

FIG. 3. (Color online) Temperature dependence of the transport resistance in BSCCO crystal B before (circles) and after (squares) current-contact irradiation at 50 and 350 Oe. Before irradiation the transport resistance is non-Ohmic (shrinking ○: I_{ac}=20,5,1, 0.1 mA, 73 Hz) due to nonuniform current flow along c axis (inset a). After contact irradiation (□) and below T_{BoG} (marked by arrows) as the current penetrates uniformly (inset b) the resistance turns Ohmic and matches that extracted from T_x(×). Below the resistive step at T_m the pristine (●) and irradiated (■) resistances are equal. Inset c: multicontact measurement of a current-contact-irradiated sample (b). Below T_{BoG}, signaled by the vanishing c-axis resistance (◇), current distributes uniformly across the sample thickness and the secondary resistance (△) equals the primary one (□).

edge impedance turns from being predominantly resistive to inductive,

$$R_e(T_x) = 2\pi f L_e, \tag{1}$$

where f is the measurement frequency. Accordingly, T_x is frequency dependent and allows sensitive determination of $R_e(T)$ down to well below the transport noise level. In its essence, this method is similar to the extraction of resistance from ac susceptibility[34,35] but with advantages of a well-defined applied current and geometry, and a direct comparison to the transport data. Yet, the main advantage lies in the spatial resolution provided by the Hall sensors which allows to distinguish between edge and bulk currents and consequently to measure separately the edge resistance for the first time.

Before doing so, the effect of the layered structure of BSCCO and the nonuniform current distribution along the c axis needs to be accounted for. At 350 Oe and f=73 Hz, for instance, we measure $T_x \simeq 58$ K. Using L_e=304 pH, calculated from sample geometry, we obtain R_e(58 K)=1.4 $\times 10^{-7}$ Ω (Fig. 3, white cross). Note, that this value is 2–3 orders of magnitude lower than the current-dependent resistance measured simultaneously in transport (open circles), which below T_{sb} should have reflected the edge resistance R_e.

Indeed, the transport resistance measured in the geometry of Fig. 3(a) has a large contribution from the c-axis resistivity, ρ_c. Due to the extreme anisotropy of BSCCO ρ_c is orders of magnitude larger than the in-plane resistivity ρ_{ab}, giving rise to nonlinearities and shear effects.[36–38] The dissipation due to ρ_c that arises from current tunneling between the CuO_2 planes, however, is not accounted in the electrodynamic considerations of the edge inductance.[33] The nonuniformity of current flow along the c axis can be remedied by introducing columnar defects solely under the current contacts [see Fig. 3(b)]. Below the Bose-glass transition, T_{BoG} (Fig. 2, diamonds), the vortices become strongly pinned to the columnar defects creating an effective electrical short along the c axis.[39–41]

This is remarkably demonstrated in a multicontact measurement of a sample irradiated in such a manner [Fig. 3(c)]. Above T_{BoG} the high anisotropy results in poor c-axis current penetration. Therefore, the primary resistance, R_p, measured on the current injecting surface, is much higher than the secondary resistance, R_s, measured on the opposite surface. At T_{BoG}, signaled by the plunging c-axis resistance R_c, the secondary resistance recovers and equals the primary.[42,43] After current-contact irradiation the resistance, measured by voltage contacts in the central pristine region of the sample, decreases by 2 orders of magnitude and turns Ohmic as demonstrated by the 0.1–20 mA curves in Fig. 3 (open squares). In contrast, the T_x temperature as measured by the Hall sensors does not involve the c-axis resistivity and hence is essentially unaffected by the contact irradiation (compare the white and black crosses in Fig. 3 before and after irradiation, respectively).

Most importantly, we find that after irradiation of the current contacts the resistive behavior becomes fully consistent with the inductive edge model. As shown below, all the data sets can be fitted by a single parameter—an effective edge inductance of L_e=490 pH (black cross in Fig. 3). This value is in a good agreement with the calculated 304 pH, considering the crude modeling of the edges taken to be round wires of diameter d.[33]

To further establish the role of the edge inductance in the T_x transition we extract $R_e(T,H)$ by repeatedly monitoring the current distribution with frequencies ranging from 1 kHz down to 0.3 Hz with resulting sensitivity of 1 nΩ (which corresponds to 1 pV sensitivity at 1 mA current). At all frequencies the in-phase component of $B^{(2)}$ rises gradually with cooling [Fig. 4(a)], as more current is shunted to the edges, until it vanishes at a frequency-dependent temperature, $T_x(f)$. The extracted edge resistance, $2\pi f L_e$ versus $T_x(f,H)$ [Fig. 4(b), circles], matches accurately the resistance measured in transport (thin lines), and extends it well below the transport noise floor. A fit to an Arrhenius behavior, $R_e(T) \sim \exp[U_e^\circ(1-T/T_c)/T]$ (dotted line), yields an edge energy barrier $U_e^\circ \sim 18T_c$.

The excellent agreement of the edge resistance extracted from $T_x(f)$ to that measured in transport confirms that the edge inductance indeed drives the electrodynamic T_x transition. Below T_x the vortex dynamics changes its character and the edge-current asymmetries disappear for the following reason. The resistive component of the edge impedance arises from dissipation due to thermal activation of vortices

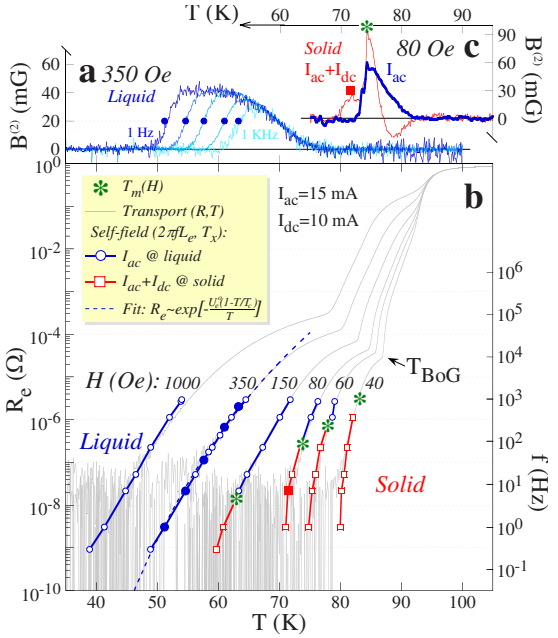

FIG. 4. (Color online) (a) Second-harmonic signals showing the frequency dependence of T_x (●). (b) It enables to extract the temperature-dependent edge resistance (○) which is thermally activated (dashed) and accurately matches the measured transport resistance (thin lines). Below melting (∗) a small dc bias is required to extract the edge resistance (□). (c) This is seen in the second-harmonic signal (thick line) that vanishes at melting (∗) but recovers with bias (thin line) before vanishing again at T_x (■).

over the surface barriers. Dissipation due to bulk vortex motion is negligible since bulk pinning is very weak and hence, $R_b \gg R_e$. Nevertheless, bulk redistribution of vortices does take place due to the presence of edge currents. With changing current polarity during the ac cycle the vortices, complying with the $B^{(1)}(x)$ Biot-Savart profile of Fig. 1(f) due to edge currents, partially shift from one side of the sample to the opposite. The resulting dB/dt reflects the inductive component of the edge impedance. At high temperatures the number of vortices redistributing from right to left during a cycle due to $dB^{(1)}(x)/dt$ is still much smaller than those that dissipatively cross the edges and move across the sample. With cooling, however, the number of vortices that cross the edges decreases exponentially and below T_x it becomes negligible compared to the number of redistributing vortices. As a result the vortices become trapped in the sample such as in a "closed box." Since in this case the total number of vortices has to be preserved, the redistribution of vortices from right to left becomes essentially purely antisymmetric and the corresponding edge currents become purely symmetric leading to disappearance of the second-harmonic signal and of the right-left asymmetry in the first harmonic. So even though the surface barriers remain asymmetric the edge currents do become symmetric since only an exponentially small fraction of vortices hop dissipatively over the barriers while most of the vortices in the "box" respond inductively. Our main finding here is that although the corresponding edge inductance is immeasurably small in transport measurements, it completely governs vortex dynamics below T_x.

Next, we use both the edge inductance at T_x as well as transport with irradiated current contacts to study the behavior of the edge resistance at the melting transition, T_m. The T_m line is measured independently by the discontinuous step in the local magnetization.[4] In the pristine sample a sharp resistive drop[44] is observed at melting (Fig. 3, solid dots). In contrast, after contact irradiation the resistive behavior is continuous (solid squares). Moreover, the two curves of pristine and contact-irradiated samples merge at the lowest measurable resistance (circled), indicating that in the presence of a uniform c-axis current distribution the edge resistance shows no sharp features. Hence, the commonly observed resistive melting drop in BSCCO apparently arises solely from a sharp drop in ρ_c.

Another intriguing feature at melting [Fig. 4(c), asterisk] is a concurrent vanishing of $B^{(2)}$ (thick line). A more detailed analysis shows that this does not result from emergent dominance of the edge inductance but rather reflects an increase in surface barriers in the vortex solid due to enhanced c-axis correlations,[32] which enhances the symmetry of the current flow. To break this enhanced symmetry below T_m and probe the edge inductance we add a small dc current bias. In its presence a finite second-harmonic signal [Fig. 4(c), thin line] subsists below melting before vanishing at T_x (square). Accordingly, the T_x line does not merge with the melting line at high temperatures as was previously believed[10] but rather bisects it at some frequency-dependent intermediate temperature.

The detection of T_x below melting allows to extract the edge resistance within the solid phase [Fig. 4(b), squares], which fits perfectly and extrapolates the transport resistance. Consequently, we find that the edge resistance measured either in transport or by the edge inductance at T_x shows no pronounced feature at melting once the c-axis contribution is removed by current-contact irradiation. This suggests that in highly anisotropic materials, such as BSCCO, the reported resistive melting step originates mostly from the loss of c-axis correlations through a simultaneous sublimation into a pancake gas.[12,18,45] In contrast, the loss of intervortex correlations within the a-b planes at melting has no significant mark in the vortex flow rate through the edges.

Finally, our complete set of data is given by dotted lines in Fig. 2 that represent contours of equal edge resistance (i.e., measured at the same frequency) spanning three and a half orders of magnitude in the H-T phase diagram. It is evident that the exponential temperature dependence of the edge resistance becomes steeper on approaching the melting as the contour lines bunch together. This is attributed to the enhanced stiffness of the pancake vortex stacks. Nevertheless, we do not find a singular behavior at melting which would have manifested itself in overlapping contour lines. On the contrary, once the c-axis contribution is eliminated the edge resistance in solid joins smoothly that of the liquid.

In summary, the spatial distribution of transport current and its frequency dependence show that the T_x line, tentatively ascribed to a phase transition of vortex matter in BSCCO, is rather an electrodynamic transition. Consequently, in the wide field and temperature range that lies

below the T_x line the inductance of the sample edges, usually dismissed in transport experiments, dominates the current flow causing ac displacement of vortices within the bulk such as in a closed box with a negligible vortex crossing of the sample edges. At T_x, the inductive part of the edge impedance equals the resistive part, which allows measurement of resistance down to 2 orders of magnitude below the transport noise. In the vicinity of the melting transition, we find that once the *c*-axis contribution is eliminated via ion irradiation of the current contacts, the edge resistance shows no sharp features at melting.

We thank H. Shtrikman for GaAs heterostructures and M. Konczykowski for ion irradiation. This work was supported by the German-Israeli Foundation (GIF). H.B. acknowledges the support of the Israel Academy of Sciences and Humanities and E.Z. the U.S.-Israel Binational Science Foundation (BSF).

*haim.beidenkopf@weizmann.ac.il

[1] G. Blatter, M. V. Feigel'man, V. B. Geshkenbein, A. I. Larkin, and V. M. Vinokur, Rev. Mod. Phys. **66**, 1125 (1994).
[2] G. P. Mikitik and E. H. Brandt, Phys. Rev. B **68**, 054509 (2003).
[3] H. Pastoriza, M. F. Goffman, A. Arribere, and F. de la Cruz, Phys. Rev. Lett. **72**, 2951 (1994).
[4] E. Zeldov, D. Majer, M. Konczykowski, V. B. Geshkenbein, V. M. Vinokur, and H. Shtrikman, Nature (London) **375**, 373 (1995).
[5] A. Schilling, R. A. Fisher, N. E. Phillips, U. Welp, W. K. Kwok, and G. W. Crabtree, Phys. Rev. Lett. **78**, 4833 (1997).
[6] H. Safar, P. L. Gammel, D. J. Bishop, D. B. Mitzi, and A. Kapitulnik, Phys. Rev. Lett. **68**, 2672 (1992).
[7] C. J. van der Beek, P. H. Kes, M. P. Maley, M. J. V. Menken, and A. A. Menovsky, Physica C **195**, 307 (1992).
[8] H. Beidenkopf, N. Avraham, Y. Myasoedov, H. Shtrikman, E. Zeldov, B. Rosenstein, E. H. Brandt, and T. Tamegai, Phys. Rev. Lett. **95**, 257004 (2005).
[9] H. Beidenkopf, T. Verdene, Y. Myasoedov, H. Shtrikman, E. Zeldov, B. Rosenstein, D. Li, and T. Tamegai, Phys. Rev. Lett. **98**, 167004 (2007).
[10] D. T. Fuchs, E. Zeldov, T. Tamegai, S. Ooi, M. Rappaport, and H. Shtrikman, Phys. Rev. Lett. **80**, 4971 (1998).
[11] A. V. Samoilov, M. V. Feigel'man, M. Konczykowski, and F. Holtzberg, Phys. Rev. Lett. **76**, 2798 (1996).
[12] L. I. Glazman and A. E. Koshelev, Phys. Rev. B **43**, 2835 (1991).
[13] B. Horovitz and T. R. Goldin, Phys. Rev. Lett. **80**, 1734 (1998).
[14] H. M. Carruzzo and C. C. Yu, Philos. Mag. B **77**, 1001 (1998).
[15] E. Frey, D. R. Nelson, and D. S. Fisher, Phys. Rev. B **49**, 9723 (1994).
[16] M. V. Feigel'man, V. B. Geshkenbein, and A. I. Larkin, Physica C **167**, 177 (1990).
[17] T. Shibauchi, T. Nakano, M. Sato, T. Kisu, N. Kameda, N. Okuda, S. Ooi, and T. Tamegai, Phys. Rev. Lett. **83**, 1010 (1999).
[18] S. Colson, M. Konczykowski, M. B. Gaifullin, Y. Matsuda, P. Gierłowski, M. Li, P. H. Kes, and C. J. van der Beek, Phys. Rev. Lett. **90**, 137002 (2003).
[19] E. Forgan, Czech. J. Phys. **46**, 1571 (1996).
[20] Y. Ando and K. Nakamura, Phys. Rev. B **59**, R11661 (1999).
[21] K. Kimura, R. Koshida, S. Okayasu, M. Sataka, Y. Kazumata, W. K. Kwok, G. W. Crabtree, and K. Kadowaki, Physica B **284-288**, 717 (2000).
[22] Yu. Eltsev, K. Nakao, S. Shibata, and N. Koshizuka, Physica C **341-348**, 1107 (2000).
[23] D. Li, P. Lin, and B. Rosenstein, Physica C **468**, 1245 (2008).
[24] J. Dietel and H. Kleinert, Phys. Rev. B **79**, 014512 (2009).
[25] R. Sugano, T. Onogi, K. Hirata, and M. Tachiki, Physica B **284-288**, 803 (2000).
[26] Y. Nonomura and X. Hu, Phys. Rev. Lett. **86**, 5140 (2001).
[27] C. P. Bean and J. D. Livingston, Phys. Rev. Lett. **12**, 14 (1964).
[28] E. Zeldov, A. I. Larkin, V. B. Geshkenbein, M. Konczykowski, D. Majer, B. Khaykovich, V. M. Vinokur, and H. Shtrikman, Phys. Rev. Lett. **73**, 1428 (1994).
[29] D. T. Fuchs, E. Zeldov, M. Rappaport, T. Tamegai, S. Ooi, and H. Shtrikman, Nature (London) **391**, 373 (1998).
[30] Y. Paltiel, D. T. Fuchs, E. Zeldov, Y. N. Myasoedov, H. Shtrikman, M. L. Rappaport, and E. Y. Andrei, Phys. Rev. B **58**, R14763 (1998).
[31] M. Konczykowski, L. I. Burlachkov, Y. Yeshurun, and F. Holtzberg, Phys. Rev. B **43**, 13707 (1991).
[32] L. Burlachkov, A. E. Koshelev, and V. M. Vinokur, Phys. Rev. B **54**, 6750 (1996).
[33] E. H. Brandt, G. P. Mikitik, and E. Zeldov, Phys. Rev. B **74**, 094506 (2006).
[34] C. J. van der Beek and P. H. Kes, Phys. Rev. B **43**, 13032 (1991).
[35] D. G. Steel and J. M. Graybeal, Phys. Rev. B **45**, 12643 (1992).
[36] R. Busch, G. Ries, H. Werthner, G. Kreiselmeyer, and G. Saemann-Ischenko, Phys. Rev. Lett. **69**, 522 (1992).
[37] B. Khaykovich, D. T. Fuchs, K. Teitelbaum, Y. Myasoedov, E. Zeldov, T. Tamegai, S. Ooi, M. Konczykowski, R. A. Doyle, and S. F. W. R. Rycroft, Phys. Rev. B **61**, R9261 (2000).
[38] V. Braude and A. Stern, Phys. Rev. B **67**, 064501 (2003).
[39] D. R. Nelson and V. M. Vinokur, Phys. Rev. Lett. **68**, 2398 (1992).
[40] M. Konczykowski, N. Chikumoto, V. M. Vinokur, and M. V. Feigelman, Phys. Rev. B **51**, 3957 (1995).
[41] T. Tamegai, N. Kameda, M. Sato, T. Shibauchi, S. Ooi, and M. Konczykowski, J. Low Temp. Phys. **117**, 1363 (1999).
[42] R. A. Doyle, W. S. Seow, Y. Yan, A. M. Campbell, T. Mochiku, K. Kadowaki, and G. Wirth, Phys. Rev. Lett. **77**, 1155 (1996).
[43] W. S. Seow, R. A. Doyle, A. M. Campbell, G. Balakrishnan, D. McK. Paul, K. Kadowaki, and G. Wirth, Phys. Rev. B **53**, 14611 (1996).
[44] D. T. Fuchs, E. Zeldov, D. Majer, R. A. Doyle, T. Tamegai, S. Ooi, and M. Konczykowski, Phys. Rev. B **54**, R796 (1996).
[45] D. T. Fuchs, R. A. Doyle, E. Zeldov, D. Majer, W. S. Seow, R. J. Drost, T. Tamegai, S. Ooi, M. Konczykowski, and P. H. Kes, Phys. Rev. B **55**, R6156 (1997).